Front. Earth Sci. 2018, 12(3): 532–544
https://doi.org/10.1007/s11707-017-0675-7

RESEARCH ARTICLE

Thermal-history reconstruction of the Baiyun Sag in the deep-water area of the Pearl River Mouth Basin, northern South China Sea

Xiaoyin TANG (✉)[1], Shuchun YANG[2], Shengbiao HU[3]

1 Geothermal and Environmental Research Laboratory, Xi'an Jiaotong University, Xi'an 710049, China
2 CNOOC Research Institute, Beijing 100027, China
3 Institute of Geology and Geophysics, Chinese Academy of Sciences, Beijing 100029, China

© Higher Education Press and Springer-Verlag GmbH Germany 2017

Abstract The Baiyun Sag, located in the deep-water area of the northern South China Sea, is the largest and deepest subbasin in the Pearl River Mouth Basin and one of the most important hydrocarbon-accumulation depression areas in China. Thermal history is widely thought to be of great importance in oil and gas potential assessment of a basin as it controls the timing of hydrocarbon generation and expulsion from the source rock. In order to unravel the paleo-heat flow of the Baiyun Sag, we first analyzed tectonic subsidence of 55 pseudo-wells constructed based on newly interpreted seismic profiles, along with three drilled wells. We then carried out thermal modeling using the multi-stage finite stretching method and calibrated the results using collected present-day vitrinite reflectance data and temperature data. Results indicate that the first and second heating of the Baiyun Sag after 49 Ma ceased at 33.9 Ma and 23 Ma. Reconstructed average basal paleo-heat flow values at the end of the rifting periods are ~57.7–86.2 mW/m^2 and ~66.7–97.3 mW/m^2, respectively. Following the last heating period at 23 Ma, the study area has undergone a persistent thermal attenuation phase, and basal heat flow has cooled down to ~64.0–79.2 mW/m^2 at present.

Keywords thermal history, tectonic subsidence, Baiyun Sag, deep-water area, South China Sea

1 Introduction

Deep-water fan systems have become primary exploration targets for increasing global petroleum output and reserves. As one of the largest deep-water sags on the northern continental slope of the South China Sea (SCS), the Baiyun Sag (BYS), with water depth of 200–2000 m, attracts attention from both oil companies and marine scientists. The first gas field, LW3-1, was found in the BYS in 2006; since then, several additional oil and gas fields/traps have been discovered. These discoveries indicate that the BYS is a region rich in oil and gas resources.

Thermal history is one of the fundamental facets of petroleum systems as it controls the timing of hydrocarbon generation and expulsion (Carminati et al., 2010; Hudson and Hanson, 2010). Although several studies have been undertaken to understand the thermal history of the BYS (Guo and He, 2007; Song et al., 2011), controversy remains regarding some issues about the thermal history, such as heating stages and the time of maximum heat flow. To date, no systematic, detailed investigations of the paleo-heat flow have been reported. In this paper, we reconstruct the thermal history of the BYS, which will provide new insights for oil and gas assessment and contribute significantly to oil and gas exploration and risk reduction.

2 Geological setting

The Pearl River Mouth Basin (PRMB), on the northern side of the SCS, is influenced by interactions of the Pacific Plate, the Eurasian Plate, and the Indian-Australian Plate (Fig. 1(a)). The BYS is the largest and deepest sag in the Zhu-II depression of the PRMB, with an area of 14,000 km^2 and maximum thickness of Cenozoic sediments over 14 km (Hu et al., 2009). It is subdivided into the main sag, the west sag, the east sag, and the south sag (Fig. 1(b)).

Received April 12, 2017; accepted August 20, 2017

E-mail: xytang2015@sina.com

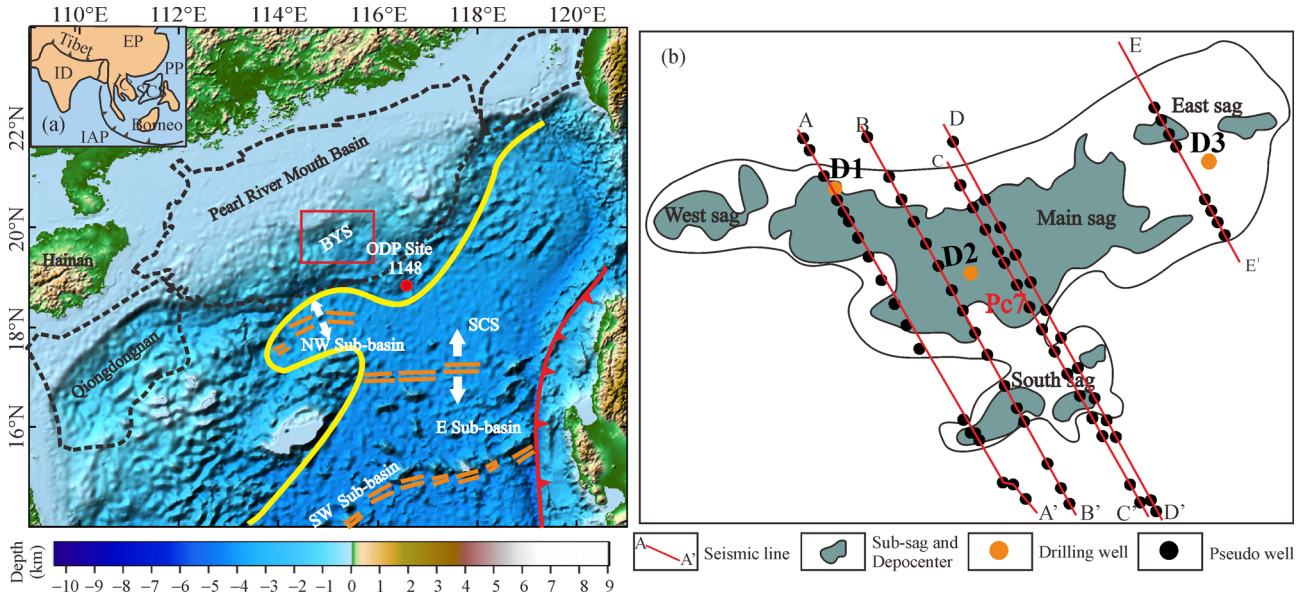

Fig. 1 (a) Location and (b) structural divisions of the Baiyun Sag (BYS). EP = Eurasian Plate, PP = Pacific Plate, ID = India, IC = Indochina, SCS = South China Sea, and IAP = Indian-Australian Plate. The red circle in (a) denotes the position of ODP Site 1148.

A general Cenozoic stratigraphic column of the deep-water area of the PRMB modified after Chen (2014) is presented in Fig. 2. The sediments change from fluvial–lacustrine–neritic shelf facies of the Paleogene syn-rift stage to deep-water slope sediments of the Neogene post-rift stage (Yan et al., 2001; Zhou et al., 2009; Zhu et al., 2012; Ding et al., 2013). The major source rocks in the PRMB were developed during the deposition of the Wenchang and Enping formations (Chen and Pei, 1993; Dai and Pang, 1999; Zhu et al., 1999). The Wenchang formation consists mainly of gray-black, organic-rich lacustrine shale with sandstone inter-beds. The Enping formation is dominated by fluvial–lacustrine–paludal shale, sandstone, and thin coal beds.

Several episodes of Cenozoic tectonic events have been recognized in the deep-water area of the PRMB (Fig. 2). These are the first and second episodes of the Zhuqiong Event at 49 Ma and 38 Ma, respectively, the Nanhai Event in the early Oligocene, the Baiyun Event (possibly related to a ridge jump) at the Paleogene/Neogene boundary, and the Dongsha Event (uplift possibly related to docking of the Philippine archipelago) in the Late Miocene (Dong et al., 2009; Zhou et al., 2009). Under the influence of multi-episode tectonic movements, the stretching/rifting process of the study area is episodic (Ru and Pigott, 1986; Zhou et al., 1995; Dong et al., 2009). The rifting stage occurred over several episodes, roughly from the Late Cretaceous or Paleogene to Early Oligocene, while the post-rifting stage has lasted roughly from the Late Oligocene to the present (Zhou et al., 2009).

3 Data and methodologies

3.1 Methods and parameters

3.1.1 Tectonic subsidence estimation

Tectonic subsidence is defined as the vertical motion (positive downward) of basement at a site that is induced by tectonic forces such as thermal contraction, tectonic deformation, and dynamic topography. In this study, the traditional back-stripping technique (Steckler and Watts, 1978; Sclater and Christie, 1980) has been used to recover the tectonic subsidence of 58 wells of the Baiyun Sag, including 55 pseudo-wells built based on seismic profiles AA'—DD' (see Fig. 1(b) for profiles' locations) and 3 drilled wells. In order to obtain tectonic subsidence information, corrections need to be made for the effects of sediment loading and compaction, changes in paleo-water depth, and global sea-level changes.

Water-loaded tectonic subsidence was determined from stratigraphic records, adopting Airy isostasy to correct for the effect of sediment loading. *In-situ* logging data from ODP Site 1148, adjacent to the study area (Fig. 1(a)), shows that the compaction history of the muddy sediments in the well follows closely that predicted by Sclater and Christie (1980) for the North Sea basin (Clift and Lin, 2001). Therefore, corrections for compaction were made using the porosity-depth relationship after Sclater and Christie (1980). The lithology of each layer is determined using as a reference the data from well D1 (Chen, 2014),

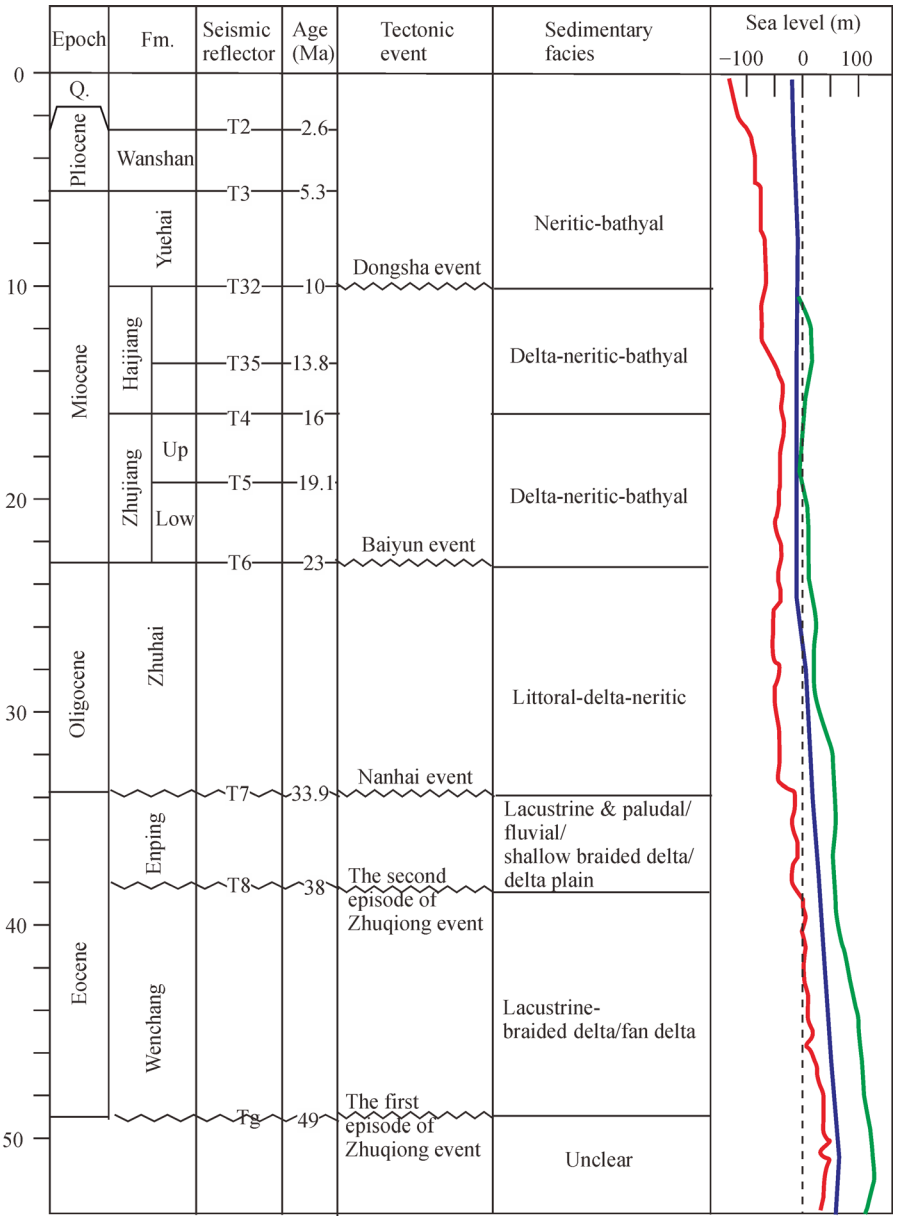

Fig. 2 Stratigraphic column, seismic reflectors, major tectonic events, sediment facies, and sea level change curves in the study area (modified after Chen, 2014). The red, blue, and green curves of sea-level change are from Cramer et al. (2009), Miller et al. (2011), and Kominz et al. (2008), respectively.

which is located on the northern edge of the Baiyun Sag (Fig. 1(b)). Estimation of paleo-water depth is difficult, yet it is essential in order to accurately study tectonic subsidence history, especially for the deep-water area (see section 4.4 for details of paleo-water analysis). Though eustatic sea-level fluctuation has less influence on back-stripping than variations in paleo-bathymetry, a recent compilation of global long-term sea-level change (Kominz et al., 2008; Cramer et al., 2009; Miller et al., 2011) has been incorporated in back-stripping to enhance subsidence-study integrity.

3.1.2 Stretching factor estimation and thermal history reconstruction

Many studies have been devoted to estimating the stretching factors in the northern margin of the SCS based on mainly three different methods, namely 1) normal faulting (e.g., Davis and Kusznir, 2004), 2) crust thinning, (e.g., Zhang et al., 2008; Zhu et al., 2016), and 3) subsidence analysis (e.g., Chen et al., 2013). The stretching factor in the first method is generally measured in the brittle upper crust simply by summing heaves on all

seismically resolvable normal faults along a profile (Westaway, 1994; Reston, 2007). Stretching-factor studies focused on crustal thinning assume that crustal-thickness variation is the consequence of crustal extension. For example, the crustal thickness of the pre-rift proto-South China Sea margin can be estimated from the present-day South China crust (Zhou et al., 2012). The present-day crustal thickness is determined from seismic detection wide-angle refraction or deep seismic reflection (Nissen et al., 1995a; Kido et al., 2001; Hu et al., 2009) or gravity modeling (Franke et al., 2011).

In contrast with the previous two methods, stretching factor from the subsidence analysis is estimated by fitting the calculated subsidence based on a given extension model and the observed subsidence (Chen, 2009). In previous publications, most of the stretching factors on the northern margin of the SCS resulting from the third method were based on either the one-stage finite stretching model (Su et al., 1989, Shi et al., 2005) or the instantaneous stretching model (Ru and Pigott, 1986; Clift and Lin, 2001). According to Jarvis and McKenzie (1980), the assumption of instantaneous extension is valid only if the stretching duration is less than 20 Ma. Thus, assessing this stretching factor in terms of either a one-stage finite stretching model or an instantaneous stretching model leads to considerable error, given that the PRMB has experienced several stages of rifting, with the entire extension lasting for over 30 Ma (Ru and Pigott, 1986; Zhou et al., 1995).

Herein, we selected a multi-stage finite stretching method (Song et al., 2011; Chen et al., 2013; Tang et al., 2014a) to assess the study area's long-term and multi-episodic extensional tectonics as well as its thermal history. This alternative approach is based on the finite stretching model proposed by Jarvis and McKenzie (1980) to avoid the problems caused by the assumption of instantaneous extension.

In this model, the theoretical tectonic subsidence is given by (Jarvis and McKenzie, 1980; White, 1994):

$$S(t) = A\left(1-\frac{1}{\beta}\right) - BQ(t), \tag{1}$$

where

$$A = \frac{t_c(\rho_m-\rho_c)}{\rho_m(1-\alpha T_m)-\rho_w}, \tag{2}$$

$$B = \frac{\alpha\rho_m}{\rho_w-\rho_m(1-\alpha T_m)}, \tag{3}$$

$$Q(t) = \int_0^a [T(z,t)-T(z,\infty)]\mathrm{d}z, \tag{4}$$

where $T(z,t)$ is the temperature of the lithosphere as a function of depth and time; $T(z,\infty)$ is the equilibrium temperature structure of the lithosphere; t_c and a are the crust and lithosphere thickness prior to stretching, respectively; ρ_w, ρ_c, and ρ_m are seawater, crust and lithospheric mantle density, respectively; α is the thermal expansion coefficient; and T_m is the lithosphere basal temperature.

The relationship between strain rate $G(t)$ and stretching factor β is

$$\beta = \exp\left(\int_0^{\Delta t} G(t)\mathrm{d}t\right). \tag{5}$$

In this model, the temperature evolution consists of rifting and its subsequent cooling phase. Temperature of the lithosphere at the rifting stage is governed by the heat conduction equation with an additional advection term:

$$\frac{\partial T}{\partial t} + G(a-z)\frac{\partial T}{\partial z} = \kappa\frac{\partial^2 T}{\partial z^2}, \tag{6}$$

where T is temperature, t is time, κ is thermal diffusivity, and $G = \dfrac{\partial u}{\partial x}$ (u is the horizontal component of velocity field) is the vertical strain rate.

Assuming the lithosphere is in thermal steady state before rifting, the temperature is given by

$$T(z,t=0^-) = T_m(1-z/a). \tag{7}$$

The boundary condition for Eq. (7) is

$$T = \begin{cases} 0, & z = a \\ T_m, & z = 0 \end{cases}. \tag{8}$$

During the rifting stage, strain rate decays exponentially with time, and reaches the value of zero at the end of rifting; that is,

$$G(t) = \begin{cases} G_0\exp(-t/\Delta\tau), & 0 \leqslant t \leqslant \Delta t_d \\ 0, & t > \Delta t_d \end{cases}, \tag{9}$$

where G_0 is the strain rate at the beginning of rifting ($t=0$), $\Delta\tau$ determines the speed of the exponential decay, and Δt_d is the stretching duration.

In the post-rift stage, the strain rate decays to zero. Lithospheric stretching ceases and the thermally perturbed lithosphere begins to cool. Thus, Eq. (6) reduces to

$$\frac{\partial T}{\partial t} = \kappa\frac{\partial^2 T}{\partial z^2}. \tag{10}$$

The heat flow is then given by

$$q(t) = -k\frac{\partial T}{\partial u}\Big|_{z=a}, \tag{11}$$

where k is the thermal conductivity.

To analyze the multi-episodic extension process, we generalize the original finite stretching model as follows.

The lithospheric temperature structure at the end of a rifting cycle, which consists of rifting and its subsequent cooling stage, is taken as the initial temperature structure of the following rifting event. In turn, the subsidence basement produced by the former rifting cycle is taken as the starting point of subsidence for the following rifting event. In terms of this structural and geothermal inheritance of the lithosphere, the following rifting event can naturally evolve from the preceding event without any pseudo intervention (Chen et al., 2013).

The procedure for modeling based on the multi-episodic finite stretching model can be briefly summarized as follows: taking into account the back-stripping/observed subsidence curves and geological information, the divisions of the syn-rift and post-rift phases are determined for each rifting event. This estimation involves calculating a number of theoretical subsidence curves using the multi-episodic finite stretching model, increasing the stretching factor by a small increment each time. The stretching factor that best fits the observed and calculated subsidence is regarded as the ideal factor for a corresponding rifting event. The cumulative stretching factor is obtained by the summation of individual stretching factors. Based on Eqs. (5), (7), (8), and (9), we can obtain the temperature evolution during the rifting stage by solving Eq. (6). Taking the temperature at the end of rifting as the initial temperature for the subsequent cooling stage, the temperature evolution during the post-rift stage can be obtained by solving Eq. (10). Finally, the thermal history can be achieved by solving Eq. (11). The related parameters used in the present study are listed and defined in Table 1.

3.2 Data and sources

3.2.1 Seismic profiles

In recent years, great effort has been devoted to investigating the deep structure of the BYS, with many multichannel seismic reflection profiles obtained and interpreted by the China National Offshore Oil Corporation (CNOOC). Those deep-penetration seismic profiles not only revealed the fine structure in the BYS but also provided us with stratigraphic information. In this study, all of the 55 pseudo-wells were built up based on 5 newly interpreted, unpublished seismic lines collected from the CNOOC. Structural and stratigraphic information for one sample profile (profile CC') is presented in Fig. 3. Seismo-stratigraphic interpretation recently carried out by the CNOOC produced the following stratigraphic horizons and ages: Tg–T8 (49–38 Ma), T8–T7(38–33.9 Ma), T7–T6 (33.9–23 Ma), T6–T5 (23–19.1 Ma), T5–T4 (19.1–16 Ma), T4–T35 (16–13.8 Ma), T35–T32 (13.8–10Ma), T32–T3 (10–5.3 Ma), and T3–seabed (5.3–0 Ma). Tg is the top of the basement, T7 approximates the Nanhai movement at 33.9 Ma, and T6 represents the Paleogene/Neogene boundary at 23 Ma. The main tectonic events and their associated seismic reflectors are shown in Fig. 2.

3.2.2 Present-day heat flow

Present-day heat flow, which can provide necessary calibration for thermal history reconstruction, is associated with the final episode of the entire scenario of basin tectono-thermal evolution, and is the only one that may be measured directly (He et al., 2001; He et al., 2002). Since the 1970s, multiple studies have reported heat-flow data from the SCS (Jessop et al., 1976; Watanabe et al., 1977; Anderson, 1980; Ru and Pigott, 1986; Matsubayashi and Nagao, 1991; Nagao et al., 1995; Nissen et al., 1995b; Xia et al., 1995; Shyu et al., 1998; He et al., 2002). He et al. (2001) systematically collected the published heat-flow data from the SCS and presented a heat-flow map with 589 data points. Based on a compilation of 592 data, Shi et al. (2003) analyzed heat-flow distribution in the SCS. Yuan et al. (2009) calculated 34 heat-flow values from the Pearl River Mouth Basin and the Qiongdongnan Basin. With 19 newly acquired heat-flow data points, Tang et al. (2014b)

Table 1 Definitions and values of parameters used in this study. STP-standard temperature and pressure. The crustal and mantle thermal conductivity are taken from He et al. (2001, 2002) and Chen (2014)

Symbol	Parameters	Value
a/km	Lithospheric thickness	125
t_c/km	Pre-rift thickness of continental crust	30
ρ_w/(kg·m^{-3})	Sea water density	1030
ρ_c/(kg·m^{-3})	Crust density at STP	2800
ρ_m/(kg·m^{-3})	Mantle density at STP	3330
T_m/°C	Temperature at base of lithosphere	1350
κ/(m^2·s^{-1})	Thermal diffusivity of lithosphere	1.0×10^{-6}
α/(°C) $^{-1}$	Lithosphere thermal expansion coefficient	3.28×10^{-5}
k_c/(W·m^{-1}·K^{-1})	Crust thermal conductivity	3.1
k_m/(W·m^{-1}·K^{-1})	Mantle thermal conductivity	2.9

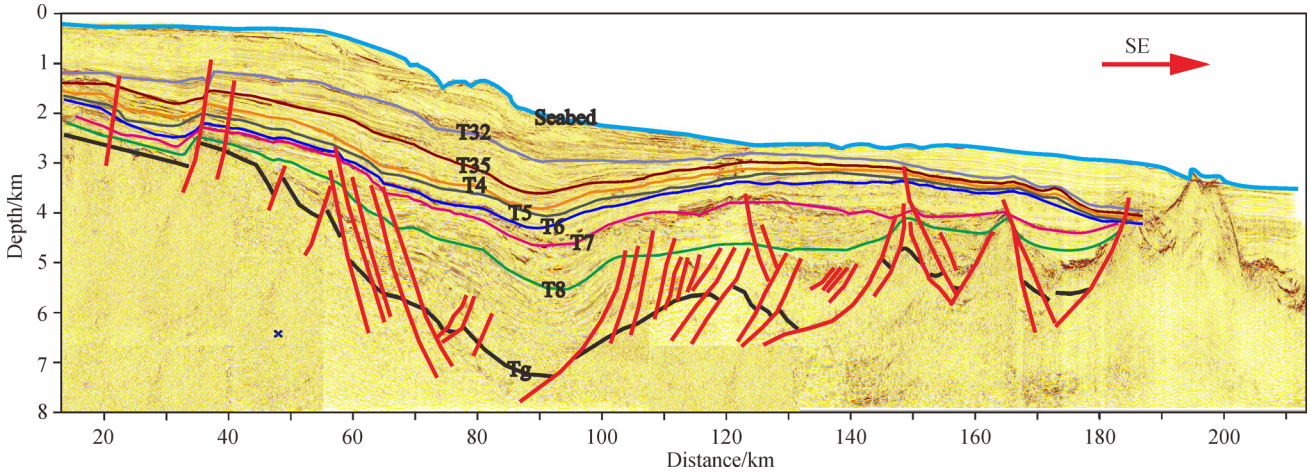

Fig. 3 One of the newly interpreted seismic section (profile CC') showing structural and stratigraphic interpretation of the BYS. The profile location is shown in Fig. 1(b) and ages of sequence boundaries are shown in Fig. 2.

demonstrated that heat-flow values in the Pearl River Mouth Basin range between 24.2 and 121 mW/m^2 with a mean value of 71.8±13.6 mW/m^2. In light of all the previous data, we found that heat flow in the Baiyun Sag is 59.2–92mW/m^2, with an average value of 79.3 mW/m^2 (Table 2).

3.2.3 Vitrinite reflectance and temperature data

Vitrinite reflectance data (Table 3) and temperature data (Table 4) of drilled wells D1, D2, and D3 (Fig. 1(b)) have been collected from the CNOOC Research Institute and used to calibrate the thermal history results (section 4.3).

Table 2 Present-day heat flow data in the Baiyun Sag collected from previous publications

Well	Depth/m	Water depth/m	Geothermal gradient/(°C·km^{-1})	Thermal conductivity/(W·m^{-1}·K^{-1})	Heat flow/(mW·m^{-2})	Source
LH29-1-2	1765–1849	764.8	53	1.67	88.4	Tang et al. (2014b)
LH29-1-1	1714–2001	723	52.1	1.64	85.3	Tang et al. (2014b)
LH29-1-3	1726–2162	1145.5	45	1.83	82.3	Tang et al. (2014b)
LH34-2-1	1770–2171	1180.5	47.4	1.77	84	Tang et al. (2014b)
LH34-2-2	1787–1888	905.8	42.8	1.79	76.6	Tang et al. (2014b)
LH34-3-1	2133–2495	1344.6	47	1.73	81.3	Tang et al. (2014b)
LW3-1-2	1775–2542	1480	43.3	1.84	79.7	Tang et al. (2014b)
LW3-1-3	1599–2199	1332.6	52.5	1.72	90.4	Tang et al. (2014b)
LW3-1-4	1802–2005	1630.2	45.5	1.87	85	Tang et al. (2014b)
LW4-1-1	1262–1837	1668.5	54	1.63	88.2	Tang et al. (2014b)
LH16-2-2	1768–1826	400	54.7	1.5	82.2	Tang et al. (2014b)
LW9-1-1	1411–1682	1668.5	53.3	1.71	91	Tang et al. (2014b)
PY33-1-1	–		35.6	2.12	75.51	Yuan et al. (2009)
LW3-1-1	–		52.5	1.75	92.00	Yuan et al. (2009)
19H	5		83	0.87	72.4	Nissen et al. (1995b)
19I	5		74	0.87	64.4	Nissen et al. (1995b)
19J	5		81	0.87	71	Nissen et al. (1995b)
19K	5		84	0.87	74	Nissen et al. (1995b)
19L	5		88	0.87	76.3	Nissen et al. (1995b)
19M	5		89	0.87	77.9	Nissen et al. (1995b)
19N	5		68	0.87	59.2	Nissen et al. (1995b)
19O	5		77	0.87	67	Nissen et al. (1995b)

Table 3 Collected vitrinite reflectance data of the drilling well D1 and D3. WS, YH, HJ, ZJ, ZH, and EP are Wanshan, Yuehai, Hanjiang, Zhujiang, Zhuhai, and Enping formations, respectively

Well	Strata	Depth/m	VRr/%	Well	Strata	Depth/m	VRr/%	Well	Strata	Depth/m	VRr/%
D1	WS	864.3	0.3	D1	ZH	3727	0.68	D1	EP	4805	1.11
D1	YH	1027	0.38	D1	ZH	3739	0.75	D1	EP	4814	1.08
D1	YH	1114	0.36	D1	ZH	3802	0.78	D1	EP	4840	1.1
D1	YH	1402	0.5	D1	ZH	3814	0.76	D1	EP	4840	1.47
D1	YH	1414	0.4	D1	ZH	3827	0.79	D1	EP	4889	1.13
D1	HJ	1577	0.36	D1	ZH	3977	0.83	D1	EP	4927	1.04
D1	HJ	1614	0.44	D1	ZH	4027	0.79	D1	EP	5039	1.19
D1	HJ	1652	0.41	D1	ZH	4039	0.77	D1	EP	5052	1.22
D1	HJ	1752	0.47	D1	ZH	4077	0.78	D1	EP	5097	1.21
D1	HJ	1852	0.47	D1	ZH	4084	0.71	D1	EP	5097	1.4
D1	HJ	1927	0.41	D1	ZH	4084	0.74	D1	EP	5112	1.27
D1	HJ	1989	0.45	D1	ZH	4089	0.79	D1	EP	5118	1.25
D1	HJ	2002	0.36	D1	ZH	4127	0.86	D1	EP	5118	1.34
D1	HJ	2177	0.5	D1	ZH	4152	0.82	D1	EP	5121	1.41
D1	HJ	2214	0.39	D1	ZH	4164	0.76	D3	HJ	2038	0.4
D1	HJ	2252	0.44	D1	ZH	4164	0.77	D3	HJ	2078	0.42
D1	HJ	2352	0.52	D1	EP	4214	0.86	D3	HJ	2118	0.4
D1	HJ	2464	0.5	D1	EP	4217	0.89	D3	HJ	2138	0.41
D1	HJ	2517	0.55	D1	EP	4225	0.92	D3	HJ	2158	0.38
D1	HJ	2564	0.5	D1	EP	4264	0.94	D3	HJ	2198	0.45
D1	ZJ	2627	0.52	D1	EP	4291	1.06	D3	ZJ	2238	0.45
D1	ZJ	2639	0.52	D1	EP	4309	0.97	D3	ZJ	2258	0.51
D1	ZJ	2727	0.48	D1	EP	4314	0.99	D3	ZJ	2298	0.49
D1	ZJ	2789	0.54	D1	EP	4318	1.12	D3	ZJ	2318	0.45
D1	ZJ	2877	0.47	D1	EP	4322	0.96	D3	ZJ	2338	0.47
D1	ZJ	2927	0.54	D1	EP	4364	0.98	D3	ZJ	2358	0.44
D1	ZJ	2939	0.55	D1	EP	4396	1.16	D3	ZJ	2398	0.47
D1	ZJ	2989	0.56	D1	EP	4402	1.11	D3	ZJ	2418	0.46
D1	ZJ	3002	0.56	D1	EP	4414	0.96	D3	ZJ	2438	0.4
D1	ZJ	3079	0.51	D1	EP	4432	1.12	D3	ZJ	2458	0.45
D1	ZJ	3089	0.56	D1	EP	4477	1.1	D3	ZJ	2478	0.43
D1	ZJ	3152	0.63	D1	EP	4489	1.03	D3	ZJ	2523	0.4
D1	ZJ	3164	0.57	D1	EP	4491	1.13	D3	ZJ	2543	0.47
D1	ZJ	3189	0.58	D1	EP	4527	1.24	D3	ZJ	2588	0.52
D1	ZJ	3276	0.63	D1	EP	4537	1.28	D3	ZH	2608	0.54
D1	ZJ	3276	0.57	D1	EP	4564	1.09	D3	ZH	2648	0.56
D1	ZJ	3327	0.58	D1	EP	4627	1.2	D3	ZH	2648	0.56
D1	ZJ	3327	0.71	D1	EP	4630	0.96	D3	ZH	2708	0.57
D1	ZJ	3389	0.66	D1	EP	4630	1.34	D3	ZH	2723	0.58
D1	ZJ	3414	0.62	D1	EP	4664	1.14	D3	ZH	2743	0.56
D1	ZJ	3464	0.65	D1	EP	4680	1.46	D3	EP	2763	0.55
D1	ZH	3564	0.65	D1	EP	4739	1.1	D3	EP	2783	0.56
D1	ZH	3639	0.65	D1	EP	4746	1.4	D3	EP	2938	0.53
D1	ZH	3689	0.74	D1	EP	4802	1.14	D3	EP	3088	0.57

Table 4 Collected temperature data of the drilling well D2. WS and ZJ are defined as the same with that in the Table 3

Well	Strata	Depth/m	Temperature/°C
D2	WS	1020	4.755
D2	ZJ	3822	130.8
D2	ZJ	3829	131.9
D2	ZJ	3836	134.1
D2	ZJ	3841	135.7
D2	ZJ	3847	136.1
D2	ZJ	3870	137.5
D2	ZJ	3953	139.3
D2	ZJ	4009	140.4
D2	ZJ	4014	141.7
D2	ZJ	4091	144.4

4 Results and discussion

4.1 Tectonic subsidence

Tectonic subsidence, which is caused solely by a tectonic driving mechanism, yields information about the regional tectonic setting and basin development. It is also a basic parameter required for calculating stretching factors and thermal history. Tectonic subsidence curves for all wells, calculated using the traditional back-stripping method (Sclater and Christie, 1980), are shown in Fig. 4. Due to the complexity of the extension process and inherent lateral heterogeneity of crust composition, it would be unrealistic to describe the subsidence history of all the wells using a uniform mode.

From section 3.1.2, we know that the division of rifting stages strongly affects heat flow reconstruction. Previous geological and geophysical investigations suggest that there are several rifting events and associated thermal activities on the northern margin of the SCS, but how the rifting stages divided and when post-rifting stages commenced is still controversial. Ru and Pigott (1986) suggested that the PRMB has experienced at least three episodic rifting phases (Late Cretaceous–Paleocene, Late Eocene–Early Oligocene, and Middle Miocene) with two intervening stages of seafloor spreading, whereas Su et al. (1989) argued that the PRMB was formed by a prolonged rifting event lasting from the Late Cretaceous to Late Oligocene with a minor event in the Middle Miocene. Song et al. (2011) suggested that the PRMB underwent two rifting episodes during the periods of 56.5–32 Ma and 32–23.3 Ma based on tectono-thermal modeling of 13 seismic profiles across this basin. The classical model of rifted-basin development suggests that the lithosphere experiences extension during the rifting stage and cooling during the post-rifting stage. The rifting and post-rifting stages are separated by a breakup unconformity, which occurred when seafloor spreading started (Falvey, 1974). Subsidence in the rifting stage depends on the stretch factor β and the duration of rifting, and post-rifting subsidence decreases exponentially according to the law of thermal contraction during lithospheric cooling (McKenzie, 1978; Jarvis and McKenzie, 1980). Seafloor magnetic anomalies indicate that the South China Sea opened at 32 Ma (Briais et al., 1993; Taylor and Hayes, 1983), or at 30 Ma according to the revised geomagnetic timescale (Cande and Kent, 1995). This event, named the Nanhai Movement (T7) by Chinese researchers (Li, 1993), was characterized by the breakup of the continental lithosphere and the inauguration of opening of the South China Sea. Under the classical model, the unconformity T7 should be regarded as the boundary between syn-rift and post-rift stages for the PRMB (Peng et al., 2005; Sun et al., 2005). Based on an analysis of subsidence in PRMB wells, Clift and Lin (2001) proposed that extension in the PRMB continued for ~5 Ma after the onset of seafloor spreading, which might imply that rifting ceased at ~25 Ma (Late Oligocene). There is an event at the Miocene/Oligocene boundary (~23.8 Ma, or ~23 Ma according to the 2013 International Chrono-stratigraphic Chart (Cohen et al., 2013)), which has been discussed in detail and named the Baiyun event (Pang et al., 2009). It was expressed as a ~3 Ma hiatus at the adjacent ODP site 1148 with abrupt changes in compositions of trace, rare-earth, and major elements (Shao et al., 2004). In the BYS, the 23.8 Ma event was also expressed by the landward jumping of the slope break, which caused a dramatic change in the sedimentary environment from littoral-deltaic to slope, accompanied by a sharp increase in sedimentation rate (Pang et al., 2009). According to Pang et al. (2009), rifting in the Baiyun Sag continued until 23.8 Ma. This is also evidenced by quantitative studies of the evolution and dynamics of the BYS conducted by Dong et al. (2009).

In this study, distinguishing the rifting stages depends on apparent changes in subsidence rate and on geologic evolution. In light of the subsidence pattern (Fig. 4) and tectonic evolution of the Baiyun sag, we consider that the first period of rifting since 49 Ma ceased at 33.9 Ma, with a deceleration at 38 Ma, while the second rifting occurred from 33.9 Ma to 23 Ma.

4.2 Thermal history

Paleo-heat flow data (Fig. 5) acquired by the multi-stage finite stretching method in this study (section 3.1.2) shows that at the end of the first stage of rifting since 49 Ma, the basal heat flow (heat flow through the base of the sedimentary basin) was increased to ~57.7–86.2 mW/m^2, then further increased to the maximum of ~66.7–97.3 mW/m^2 at the end of the following rifting stage (~23 Ma). Finally, the basin cooled down to present-day basal heat flow, with a value of ~64.0–79.2 mW/m^2. Sedimentary thickness of all the wells for modeling ranges

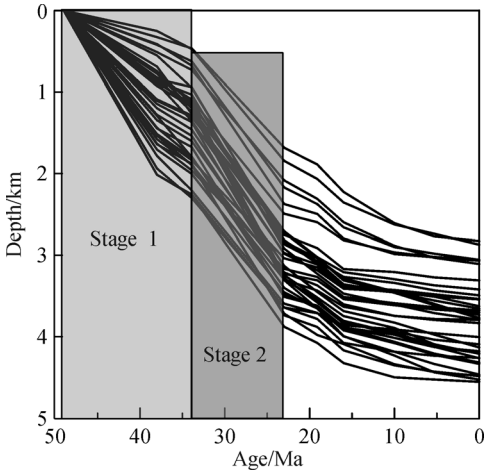

Fig. 4 An overview of the back-stripped tectonic subsidence curves for all the wells. Gray-shaded regions show the inferred rifting stages.

from 1.6 km to 9.5 km. Given the average radiogenic heat production rate of 1.28 μW/m^3 (He et al., 2002; Yuan et al., 2009), the surface heat flow of the Baiyun Sag is about 67.7–90.2 mW/m^2, which is consistent with the published present-day heat flow value of 59.2–92 mW/m^2 (Table 2).

According the results of this study, the BYS underwent continuous heating from 49 Ma to 23 Ma, and then began to experience a thermal attenuation phase.

4.3 Result calibration

Vitrinite refrectance and temperature data are two commonly used indicators for calibration of the reconstructed thermal history (Rodon and Littke, 2005; Zuo et al., 2015). Given the thermal history acquired from this study, we calculated vitrinite reflectance and temperature using the "Genesis" program (version 4.91, ZetaWare, Inc.). For the calculation of vitrinite reflectance, the EASY %Ro algorithm of Sweeney and Burnham (1990) was selected. A good agreement between calculated and measured values of vitrinite reflectance and temperatures is displayed in Fig. 6, which implies that the reconstructed thermal history in this study is reasonable. Unfortunately, we could not accumulate both the vitrinite reflectance data and temperature data for the same well because of the paucity of exploration in the study area.

4.4 Paleo-bathymetry

Because the study region is situated on the continental slope, where the maximum present-day bathymetry exceeds 2000 m, its paleo-bathymetry potentially has an important effect in back-stripping and deserves particular attention. A number of sources, such as benthic microfossils, faunal and floral assemblages, sedimentary facies, and distinctive geochemical signatures, can provide information about paleo-bathymetry, but reliable estimates usually come from bio-stratigraphic data from wells (Bessis, 1986; Allen and Allen, 2013). Unfortunately, no drilled well with paleontological data is available in the Baiyun Sag to date. ODP Site 1148, with present water depth of 3294 m, is located near the study area. Wang et al. (2000) reported that the Early Oligocene sediments recovered from ODP Site 1148 are of deep-water facies, and this deep-water sequence likely continues downward in the seismic profile, indicative of the occurrence of a deep-water environment in the northern slope at least since the Early Oligocene and probably even earlier (Wang et al., 2003; Wang, 2012). Detailed study of benthic faunas from ODP Site 1148 shows an obvious change in water depth from the upper bathyal zone shallower than 1000 m in the earliest Oligocene (ca. 33.5–32 Ma) to 1000–1500 m in the late early Oligocene (ca. 32–27 Ma), lower bathyal zone between 1500 m and 2500 m in the late Oligocene to earlier middle Miocene (ca. 26–14 Ma), and depths similar to the present day (2500–3500 m) since the late middle

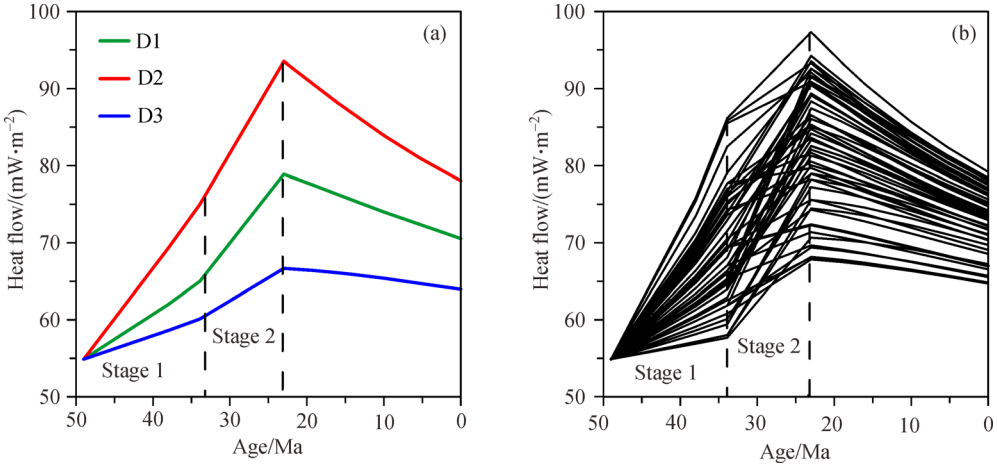

Fig. 5 Reconstructed thermal history of the Baiyun Sag, (a) for drilled wells and (b) for pseudo-wells.

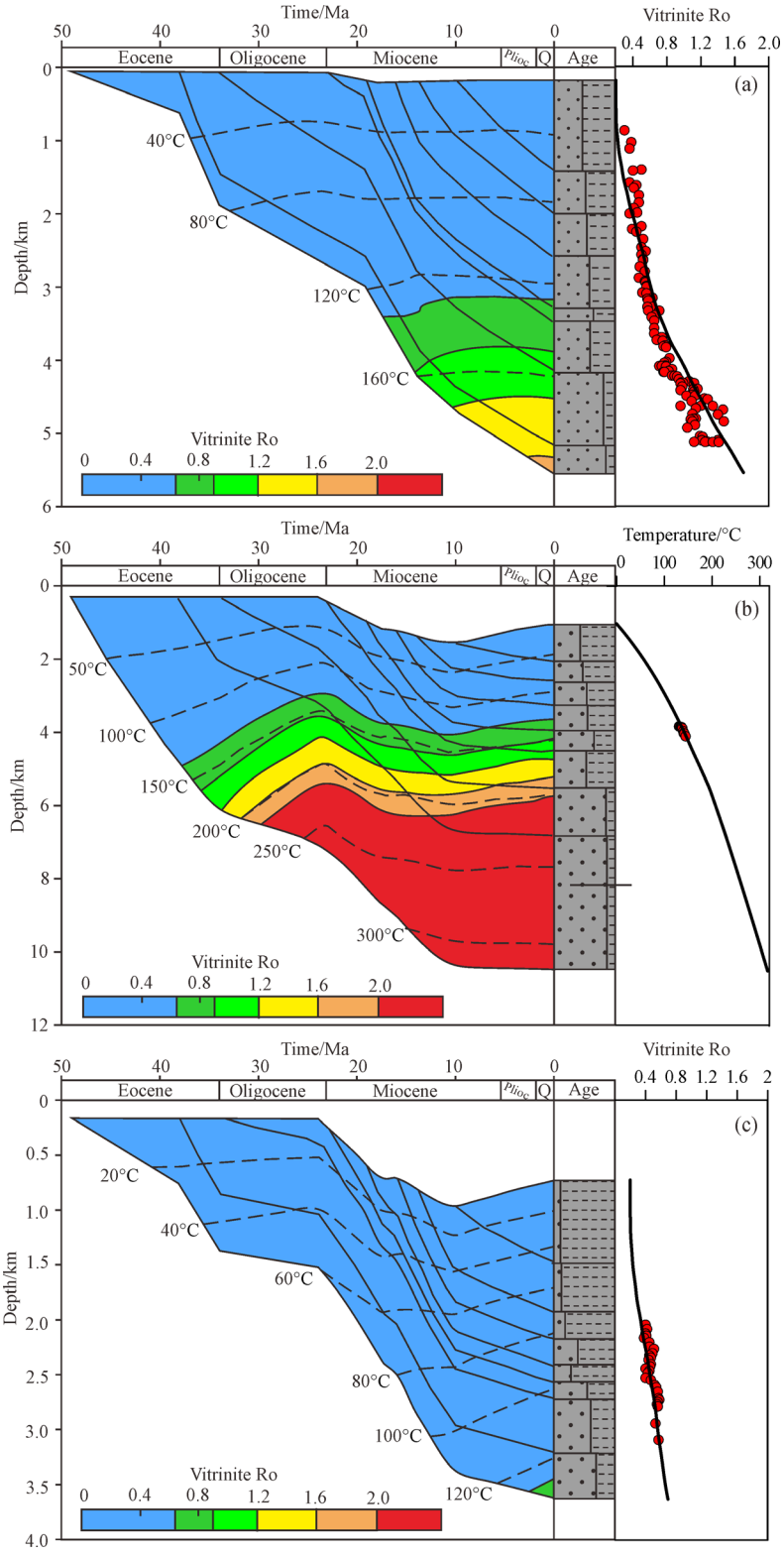

Fig. 6 Burial history, temperature history, and thermal maturity history for the drilled wells, D1 (a), D2 (b), D3 (c). To the right, the depth vs. temperature or/and depth vs. mean vitrinite reflectance data are presented, showing a good fit between observed data (plotted in solid red circles) and modeled data (solid black line).

Miocene (14 Ma to the present) (Zhao, 2005). Pang et al. (2007) reported a similar trend in the sedimentary sequence from the Baiyun Sag, indicating a transition from shallow to deep water conditions during this time span. Keeping the above information in mind, here we estimate paleo-bathymetry according to the following assumptions: 1) seafloor depth defined by seismic profiles accurately gives present-day bathymetry for any given site; 2) water depth at Tg (basement) (i.e., 49 Ma) is assumed to be zero; 3) estimates for the pseudo-wells are constrained by the water-depth trend from ODP Site 1148 assessed by Zhao (2005). The present water depth is 3294 m at ODP Site 1148 (Shipboard Scientific Party, 2000). In light of the paleo-water trend of this site described by Zhao (2005), we can set the paleo-water depth of this site at 10 Ma to 2700 m, at 23 Ma to 1700 m, at 33.9 Ma to 800 m, at 49 Ma to 0 m. Thus, after we obtain the present water depth, we can finally derive the paleo-water trend of the pseudo-well in accordance with the similar trend of ODP Site 1148. For example, the present water depth of pseudo-well Pc7 (Fig. 1(b)) is 1605 m, resulting from the seismic profile explanation. According to the water-depth trend of ODP Site 1148, we can set the paleo-water depth to 1315 m at 10 Ma, 828 m at 23 Ma, and 389 m at 33.9 Ma. Paleo-water depths at other ages of this well can be determined by linear interpolation.

5 Conclusions

After 49 Ma, the first rifting of the Baiyun Sag ceased at 33.9 Ma, and the second rifting lasted from ~33.9 to 23 Ma. In response to these rifting stages, the Baiyun Sag has experienced two heating phases and a subsequent persistent cooling through the present. From 49 Ma to 33.9 Ma, the average basal heat flow increased from ~54.9 to ~69.9 mW/m^2; the second heating phase lasted from ~33.9 Ma to 23 Ma, resulting in an increase in average basal heat flow from ~69.9 to ~82. 6 mW/m^2. Finally, the Baiyun Sag cooled down to its present thermal state, with a decrease in average basal heat flow from ~82.6 to ~72.9 mW/m^2.

Acknowledgements Research in this paper was supported by the National Natural Science Foundation of China (Grant No. 41602251), the Chinese Postdoc Fund, No.58 General Fund, 2015 (No. 2015M582636) and the Research Fund for New Teachers of Xi'an Jiaotong University. We are grateful to CNOOC Research Institute for providing the seismic profiles. We also thank anonymous reviewers for their careful and insightful suggestions on the paper.

References

Allen P A, Allen J R (2013). Basin Analysis: Principles and Application to Petroleum Play Assessment. John Wiley & Sons

Anderson R N (1980). 1980 Update of Heat Flow in the East and Southeast Asian Seas. AGU: 319–326

Bessis F (1986). Some remarks on the study of subsidence of sedimentary basins application to the Gulf of Lions margin (Western Mediterranean). Mar Pet Geol, 3(1): 37–63

Briais A, Patriat P, Tapponnier P (1993). Updated interpretation of magnetic anomalies and seafloor spreading stages in the South China Sea: implications for the Tertiary tectonics of Southeast Asia. J Geophys Res B Solid Earth, 98(B4): 6299–6328

Cande S C, Kent D V (1995). Revised calibration of the geomagnetic polarity timescale for the Late Cretaceous and Cenozoic. J Geophys Res, 10(B4): 6093–6095

Carminati E, Cavazza D, Scrocca D, Fantoni R, Scotti P, Doglioni C (2010). Thermal and tectonic evolution of the southern Alps (northern Italy) rifting: coupled organic matter maturity analysis and thermokinematic modeling. AAPG Bull, 94(3): 369–397

Chen L (2009). Numerical modeling study of the rifted continental margin of the South China Sea. Dissertation for PhD degree. Institute of Geology and Geophysics, Chinese Academy of Sciences, Beijing, China, 1–165 (in Chinese)

Chen L (2014). Stretching factor estimation for the long-duration and multi-stage continental extensional tectonics: application to the Baiyun Sag in the northern margin of the South China Sea. Tectonophysics, 611(0): 167–180

Chen L, Zhang Z, Song H (2013). Weak depth and along-strike variations in stretching from a multi-episodic finite stretching model: evidence for uniform pure-shear extension in the opening of the South China Sea. J Asian Earth Sci, 78: 358–370

Chen S, Pei C (1993). Geology and geochemistry of source rocks of the eastern Pearl River mouth basin, South China Sea. J Asian Earth Sci, 8(1): 393–406

Clift P, Lin J (2001). Preferential mantle lithospheric extension under the South China margin. Mar Pet Geol, 18(8): 929–945

Cohen K, Finney S, Gibbard P (2013). International Chronostratigraphic Chart v 2013/01. International Commission on Stratigraphy

Cramer B S, Toggweiler J R, Wright J D, Katz M E, Miller K G (2009). Ocean overturning since the Late Cretaceous: inferences from a new benthic foraminiferal isotope compilation. Paleoceanography, 24(4): PA4216

Dai Y, Pang X (1999). Petroleum geological characteristics of the Zhu II Depression, Pearl River Mouth Basin. China Offshore Oil and Gas, 13(3): 169–173 (in Chinese)

Davis M, Kusznir N (2004). Depth-dependent lithospheric stretching at rifted continental margins. Proceedings of NSF Rifted Margins Theoretical Institute, 136: 92

Ding W, Franke D, Li J, Steuer S (2013). Seismic stratigraphy and tectonic structure from a composite multi-channel seismic profile across the entire Dangerous Grounds, South China Sea. Tectonophysics, 582(0): 162–176

Dong D, Zhang G, Zhong K, Yuan S, Wu S (2009). Tectonic evolution and dynamics of deepwater area of Pearl River Mouth Basin, Northern South China Sea. J Earth Sci, 20(1): 147–159

Falvey D A (1974). The development of continental margins in plate tectonic theory. Am Assoc Pet Geol Bull, 14(1): 95–106

Franke D, Barckhausen U, Baristeas N, Engels M, Ladage S, Lutz R, Montano J, Pellejera N, Ramos E G, Schnabel M (2011). The

continent-ocean transition at the southeastern margin of the South China Sea. Mar Pet Geol, 28(6): 1187–1204

Guo X, He S (2007). Source rock thermal and maturity history modeling in the Baiyun sag of the Pearl River Mouth basin. Petroleum Geology and Experiment, 29(4): 420–425 (in Chinese)

He L, Wang K, Xiong L, Wang J (2001). Heat flow and thermal history of the South China Sea. Phys Earth Planet Inter, 126(3–4): 211–220

He L, Xiong L, Wang J (2002). Heat flow and thermal modeling of the Yinggehai Basin, South China Sea. Tectonophysics, 351(3): 245–253

Hu D, Zhou D, Wu X, He M, Pang X, Wang Y (2009). Crustal structure and extension from slope to deepsea basin in the northern South China Sea. J Earth Sci, 20(1): 27–37

Hudson S M, Hanson A D (2010). Thermal maturation and hydrocarbon migration within La Popa Basin, northeastern Mexico, with implications for other salt structures. AAPG Bull, 94(3): 273–291

Jarvis G T, McKenzie D P (1980). Sedimentary basin formation with finite extension rates. Earth Planet Sci Lett, 48(1): 42–52

Jessop A M, Hobart M A, Sclater J G (1976). The world heat flow data collection 1975. Geothermal Series Number 5, Earth Physics Branch, Energy, Mines and Resources, Ottawa, Canada

Kido Y, Suyehiro K, Kinoshita H (2001). Rifting to spreading process along the northern continental margin of the South China Sea. Mar Geophys Res, 22(1): 1–15

Kominz M A, Browning J V, Miller K G, Sugarman P J, Mizintseva S, Scotese C R (2008). Late Cretaceous to Miocene sea-level estimates from the New Jersey and Delaware coastal plain coreholes: an error analysis. Basin Res, 20(2): 211–226

Li P (1993). Cenozoic tectonic movement in the Pearl River Mouth Basin. China Offshore Oil Gas (Geol), 7(6): 11–17 (in Chinese)

Matsubayashi O, Nagao T (1991). Compilation of heat flow data in southeast Asia and its marginal seas. In: Cermak V, Rybach L, eds. Terrestrial Heat Flow and the Lithosphere Structure. Berlin: Springer, 445–456

McKenzie D (1978). Some remarks on the development of sedimentary basins. Earth Planet Sci Lett, 40(1): 25–32

Miller K G, Mountain G S, Wright J D, Browning J V (2011). A 180-million-year record of sea level and ice volume variations from continental margin and deep-sea isotopic records. Oceanography (Wash DC), 24(2): 40–53

Nagao T, Uyeda S, Matsubayashi O (1995). Overview of heat flow distribution in Asia based on the IHFC compilation with special emphasis on south-east Asia. In: Gupta M L, Yamano M, eds. Terrestrial Heat Flow and Geothermal Energy in Asia. Rotterdam: A. A. Balkema, 221–238

Nissen S S, Hayes D E, Bochu Y, Weijun Z, Yongqin C, Xiaupin N (1995b). Gravity, heat flow, and seismic constraints on the processes of crustal extension: northern margin of the South China Sea. J Geophys Res, 100(B11): 22447–22483

Nissen S S, Hayes D E, Buhl P, Diebold J, Bochu Y, Zeng W, Chen Y (1995a). Deep penetration seismic soundings across the northern margin of the South China Sea. J Geophys Res Solid Earth, 100 (B11): 22407–22433

Pang X, Chen C, Shao L, Wang C, Zhu M, He M, Shen J, Lian S, Wu X (2007). Baiyun Movement, a great tectonic event on the Oligocene–Miocene boundary in the northern South China Sea and its implications. Geological Review, 53(2): 145–151 (in Chinese)

Pang X, Chen C, Zhu M, He M, Shen J, Lian S, Wu X, Shao L (2009). Baiyun movement: a significant tectonic event on Oligocene/Miocene boundary in the northern South China Sea and its regional implications. J Earth Sci, 20(1): 49–56

Peng D J, Pang X, Chen C M, Shu Y, Ye B, Gan Q G, Wu C R, Huang X L (2005). From shallow-water shelf to deep-water slope—The study on deep-water fan systems in South China Sea. Acta Sedimentologica Sinica, 23(1): 1–11 (in Chinese)

Reston T (2007). Extension discrepancy at North Atlantic nonvolcanic rifted margins: depth-dependent stretching or unrecognized faulting? Geology, 35(4): 367–370

Rodon S, Littke R (2005). Thermal maturity in the Central European Basin System (Schleswig-Holstein area): results of ID basin modelling and new coalification maps. Int J Earth Sci (Geol Rundsch), 94(5–6): 815–883

Ru K, Pigott J D (1986). Episodic rifting and subsidence in the South China Sea. AAPG Bull, 70(9): 1136–1155

Sclater J G, Christie P A F (1980). Continental stretching: an explanation of the post-Mid-Cretaceous subsidence of the central North Sea Basin. J Geophys Res, 85(NB7): 3711–3739

Shao L, Li X H, Wang P X, Jian Z M, Wei G J, Pang X, Liu Y (2004). Sedimentary record of the tectonic evolution of the South China Sea since the Oligocene: evidence from deep sea sediments of ODP Site 1148. Advances in Earth Science, 19(4): 539–544 (in Chinese)

Shi X B, Burov E, Leroy S, Qiu X L, Xia B (2005). Intrusion and its implication for subsidence: a case from the Baiyun Sag, on the northern margin of the South China Sea. Tectonophysics, 407(1–2): 117–134

Shi X, Qiu X, Xia K, Zhou D (2003). Characteristics of surface heat flow in the South China Sea. J Asian Earth Sci, 22(3): 265–277

Shipboard Scientific Party (2000). Leg 184 summary: exploring the Asian monsoon through drilling in the South China Sea. In: Wang P, Prell W, Blum P, eds. Proceedings of the ODP, Initial Results. IODP, College Station, TX. 1–77

Shyu C T, Hsu S K, Liu C S (1998). Heat flows off southwest Taiwan: measurements over mud diapirs and estimated from bottom simulating reflectors. Terrestrial Atmospheric & Oceanic Sciences, 9(4): 795–812

Song Y, Zhao C, Zhang G, Song H, Shan J, Chen L (2011). Research on tectono-thermal modeling for Qiongdongnan Basin and Pearl River Mouth Basin in the northern South China Sea. Chin J Geophys, 54: 3057–3069 (in Chinese)

Steckler M, Watts A (1978). Subsidence of the Atlantic-type continental margin off New York. Earth Planet Sci Lett, 41(1): 1–13

Su D, White N, McKenzie D A N (1989). Extension and subsidence of the Pearl River Mouth Basin, northern South China Sea. Basin Res, 2 (4): 205–222

Sun Z, Pang X, Zhong Z H (2005). Dynamics of tertiary tectonic evolution of the Baiyun Sag in the Pearl River Mouth Basin. Earth Sci Front, 12(4): 489–498

Sweeney J J, Burnham A K (1990). Evaluation of a simple-model of vitrinite reflectance based on chemical-kinetics. AAPG Bull, 74(10): 1559–1570

Tang X, Chen L, Hu S, Yang S, Zhang G, Shen H, Rao S, Li W (2014a). Tectono-thermal evolution of the Reed Bank Basin, Southern South

China Sea. J Asian Earth Sci, 96: 344–352

Tang X Y, Hu S B, Zhang G C, Yang S C, Shen H L, Rao S, Li W W (2014b). Characteristic of surface heat flow in the Pearl River Mouth Basin and its relationship with thermal lithosphere thickness. Chin J Geophys, 57(6): 1857–1867

Taylor B, Hayes D E (1983). Origin and history of the South China basin. In: Hayes D E, ed. The Tectonics and Geological Evolution of Southeast Asia Seas and Islands, Part 2. Geophysics Monographs Series, AGU, Washington, D.C., 27: 23–56

Wang P (2012). Tracing the life history of a marginal sea—on "The South China Sea Deep" research program. Chin Sci Bull, 57(24): 3093–3114

Wang P, Blum P, Nessler S (2000). Proceedings of the Ocean Drilling Program, Inital Reports, vol. 184. http://www.ldeo.columbia.edu

Wang P, Jian Z, Zhao Q, Li Q, Wang R, Liu Z, Wu G, Shao L, Wang J, Huang B (2003). Evolution of the South China Sea and monsoon history revealed in deep-sea records. Chin Sci Bull, 48(23): 2549–2561

Watanabe T, Langseth M G, Anderson R N (1977). Heat flow in back-arc basins of the western Pacific. In: Talwani M, Pitman W C, eds. Island Arcs, Deep Sea Trenches and Back-Arc Basins. AGU, Washington, D.C., 137–167

Westaway R (1994). Re-evaluation of extension across the Pearl River Mouth Basin, South China Sea-implications for continental lithosphere deformation mechanisms. J Struct Geol, 16(6): 823–838

White N (1994). An inverse method for determining lithospheric strain rate variation on geological timescales. Earth Planet Sci Lett, 122(3–4): 351–371

Xia K, Xia S, Chen Z (1995). Geothermal characteristics of the South China Sea. In: Gupta M L, Yamano M, eds. Terrestrial Heat Flow and Geothermal Energy in Asia. New Delhi: IBH Publishing Co. Pvt Ltd, 113–128

Yan P, Zhou D, Liu Z (2001). A crustal structure profile across the northern continental margin of the South China Sea. Tectonophysics, 338(1): 1–21

Yuan Y, Zhu W L, Mi L J, Zhang G C, Hu S B, He L J (2009). "Uniform geothermal gradient" and heat flow in the Qiongdongnan and Pearl River Mouth Basins of the South China Sea. Mar Pet Geol, 26(7): 1152–1162

Zhang Y, Sun Z, Zhou D, Guo X, Shi X, Wu X, Pang X (2008). Stretching characteristics and its dynamic significance of the northern continental margin of South China Sea. Sci China Ser D Earth Sci, 51(3): 422–430

Zhao Q (2005). Late Cainozoic ostracod faunas and paleoenvironmental changes at ODP Site 1148, South China Sea. Mar Micropaleontol, 54 (1): 27–47

Zhou D, Ru K, Chen H Z (1995). Kinematics of Cenozoic extension on the South China Sea continental margin and its implications for the tectonic evolution of the region. Tectonophysics, 251(1–4): 161–177

Zhou D, Sun Z, Liao J, Zhao Z, He M, Wu X, Pang X (2009). Filling history and post-breakup acceleration of sedimentation in Baiyun sag, deepwater northern South China Sea. J Earth Sci, 20(1): 160–171

Zhou L, Xie J, Shen W, Zheng Y, Yang Y, Shi H, Ritzwoller M H (2012). The structure of the crust and uppermost mantle beneath South China from ambient noise and earthquake tomography. Geophys J Int, 189(3): 1565–1583

Zhu J, Li J, Sun Z, Li S (2016). Crustal thinning and extension in the northwestern continental margin of the South China Sea. Geol J, 51 (S1): 286–303

Zhu J, Qiu X, Kopp H, Xu H, Sun Z, Ruan A, Sun J, Wei X (2012). Shallow anatomy of a continent–ocean transition zone in the northern South China Sea from multichannel seismic data. Tectonophysics, 554: 18–29

Zhu W, Li M, Wu P (1999). Petroleum systems of the Zhu III subbasin, Pearl River Mouth Basin, South China Sea. AAPG Bulletin-American Association of Petroleum Geologists, 83(6): 990–1003

Zuo Y H, Qiu N S, Pang X Q, Li J W, Hao Q Q, Chang J (2015). Meso-Cenozoic Tectono-thermal evolution history in Bohai Bay Basin, North China. J Earth Sci, 26(3): 352–360